INSTITUTE OF PHYSICS PUBLISHING and INTERNATIONAL ATOMIC ENERGY AGENCY NUCLEAR FUSION

Nucl. Fusion **46** (2006) L9–L12 doi:10.1088/0029-5515/46/8/L03

LETTER

Shielding of the error field by a liquid metal wall in tokamaks

L.-J. Zheng, M. Kotschenreuther and F.L. Waelbroeck

Institute for Fusion Studies, University of Texas at Austin, Austin, TX 78712

E-mail: lzheng@mail.utexas.edu

Received 12 October 2005, accepted for publication 22 June 2006
Published 25 July 2006
Online at stacks.iop.org/NF/46/L9

Abstract
It is shown that the error field in a tokamak can be shielded by a flowing liquid metal wall. In particular, a flowing liquid metal wall can prevent resonance amplification of the error field by the plasma near its no-wall stability limit.

PACS numbers: 52.35.Py, 52.55.Fa, 52.55.Hc

The resistive wall mode stability is an issue of concern for tokamak confinement [1]. Experimentally, it was observed that plasma rotation can stabilize resistive wall modes [2–4]. Theoretically, it was found that mode coupling to the sound wave and to the shear Alfvén resonances in rapidly rotating plasmas can lead to stabilization of the resistive wall modes [5–7]. Unfortunately, recent experiments in DIII-D show that the rotation damps even in the presence of continuous unbalanced neutral beam injection [3]. This indicates that there is a strong braking torque that slows down the plasma rotation. Theoretically, an error field amplification mechanism has been proposed to explain the rotation braking [8, 9]. Error-field-induced rotation braking has been verified experimentally [10]. When the error field is reduced, the plasma rotation is found to last longer. A review of various theoretical models has been given in [11].

In this letter, we propose an alternative approach to ameliorate the effects of the error field. We show that the error field, which is otherwise amplified, can be shielded by a flowing liquid metal wall. In particular, we prove that the strongly peaked torque barrier on the plasma rotation at the no-wall stability limit can be removed by a flowing liquid metal wall. To investigate the shielding effect from a liquid metal wall, we use a thin-wall approximation and model the error field by a thin current-carrying layer. Without loss of generality, the error-field current layer is assumed to be located immediately outside the liquid metal wall. The system is as follows: the plasma torus is surrounded by an inner vacuum region; the inner vacuum region is enclosed by a thin liquid metal wall; immediately outside the liquid metal wall is a thin error-field current layer, and outside the error-field current layer is an outer vacuum region, which extends to infinity. We use the coordinate system (ψ, θ, ϕ), where ψ represents the radial coordinate, θ is the poloidal angle and ϕ is the axisymmetric toroidal angle. The equilibrium magnetic field is expressed as $\vec{B} = \nabla\phi \times \nabla\psi + g(\psi)\nabla\phi$. The Jacobian of this coordinate system is $\mathcal{J} = 1/(\nabla\psi \times \nabla\theta \cdot \nabla\phi)$. Let ψ_a, ψ_{b-}, ψ_b and ψ_{b+} designate the radial locations for the interface between the plasma and the inner vacuum region, the interface between the inner vacuum region and the liquid metal wall, the interface between the liquid metal wall and the error-field current layer, and the interface between the error-field current layer and outside vacuum region, respectively.

Since the error field is small compared with the toroidally axisymmetric equilibrium field, linear perturbation theory can be used to evaluate its effect. The solution procedure is as follows: we first describe the solutions in the vacuum and plasma regions. These solutions are then matched to each other across the various interfaces. Instead of calculating the torque on the plasma, we calculate the torque on the wall and the error-field current layer; this is opposite to the torque on the plasma that causes braking of plasma rotation.

For the sake of conciseness, we outline the general solutions for the inner and outer vacuum regions simultaneously. The vacuum regions are described by the Laplace equation

$$\nabla^2 u = 0, \tag{1}$$

where u is the magnetic scalar potential and is related to the perturbed magnetic field by $\delta\vec{B} = -\nabla u$. To solve equation (1), Fourier decompositions are introduced for both poloidal and toroidal coordinates: $u = 1/\sqrt{2\pi}\sum_m u_m \exp\{\mathrm{i}(m\theta - n\phi)\}$, where n is the toroidal mode number. Suppose only M harmonics are kept in the poloidal decomposition, then equation (1) becomes a set of second-order differential equations of number M. This set of second-order differential equations can be

transformed into a set of first-order differential equations of number $2M$, by introducing a new field $v = -\mathcal{J}\nabla\psi\cdot\delta\vec{B}$. The new field v is related to the magnetic scalar potential in Fourier space as follows:

$$\langle v\rangle = [[\mathcal{J}|\nabla\psi|^2]]\frac{\partial\langle u\rangle}{\partial\psi} + [[i\mathcal{J}\nabla\psi\cdot\nabla\theta]]\mathcal{M}\langle u\rangle,$$

where $\mathcal{M}$ is a $M\times M$ matrix with its components defined as $\mathcal{M}_{mm'} = m\delta_{mm'}$ with $\delta_{mm'}$ the Kronecker delta, $\langle\cdots\rangle$ denotes the vector in Fourier space corresponding to a quantity (i.e. a single column matrix with M Fourier components as elements), and $[[\cdots]]$ represents the $M\times M$ matrix that corresponds to a quantity with its components defined as follows:

$$[[\cdots]]_{mm'} = \frac{1}{2\pi}\int_{-\pi}^{\pi} \mathrm{d}\theta \mathrm{e}^{-im\theta}(\cdots)\mathrm{e}^{im'\theta}.$$

After Fourier decomposition there are $2M$ independent solutions for equation (1), namely, $\begin{pmatrix}\langle u\rangle^k\\ \langle v\rangle^k\end{pmatrix}$ with $k = 1,\cdots,2M$. These independent solutions are used to construct the following independent solution matrices:

$$\begin{pmatrix}\mathcal{U}_1\\ \mathcal{V}_1\end{pmatrix} \equiv \begin{pmatrix}\langle u\rangle^1,\ldots,\langle u\rangle^M\\ \langle v\rangle^1,\ldots,\langle v\rangle^M\end{pmatrix},$$
$$\begin{pmatrix}\mathcal{U}_2\\ \mathcal{V}_2\end{pmatrix} \equiv \begin{pmatrix}\langle u\rangle^{M+1},\ldots,\langle u\rangle^{2M}\\ \langle v\rangle^{M+1},\ldots,\langle v\rangle^{2M}\end{pmatrix}.$$

The general solutions in the vacuum regions can be expressed as a linear combination of the independent solutions:

$$\begin{pmatrix}\langle u\rangle\\ \langle v\rangle\end{pmatrix} = \begin{pmatrix}\mathcal{U}_1\\ \mathcal{V}_1\end{pmatrix}\boldsymbol{c}_v + \begin{pmatrix}\mathcal{U}_2\\ \mathcal{V}_2\end{pmatrix}\boldsymbol{d}_v, \tag{2}$$

where $\boldsymbol{c}_v$ and $\boldsymbol{d}_v$ are constant vectors in the independent solution space (i.e. single column matrices with M constants as their elements). To distinguish the inner and outer vacuum solutions, we let $\boldsymbol{c}_{v1}$ and $\boldsymbol{d}_{v1}$ denote the constants for the inner vacuum region and $\boldsymbol{c}_{v2}$ and $\boldsymbol{d}_{v2}$ for the outer vacuum region.

In the outer vacuum region, the scalar potential $\langle u\rangle$ is subjected to M boundary conditions at infinite ψ. With these M boundary conditions imposed, there are only M independent solutions left. Without loss of generality, we can set $\boldsymbol{c}_{v2}$ to be zero in this case. Consequently, eliminating $\boldsymbol{d}_{v2}$ in equation (2), we obtain

$$\langle u\rangle|_{\psi_{b+}} = \mathcal{T}\langle v\rangle|_{\psi_{b+}}, \tag{3}$$

where the $M\times M$ matrix $\mathcal{T}$ is given by $\mathcal{T} = \mathcal{U}_2\mathcal{V}_2^{-1}|_{\psi_{b+}}$. The matrix $\mathcal{T}$ can be computed by means of the Green function method [12].

In the inner vacuum region, the independent solutions can be constructed, for example, with the use of an inward numerical shooting [13], for the following boundary conditions at ψ_{b-}:

$$\begin{pmatrix}\mathcal{U}_1\\ \mathcal{V}_1\end{pmatrix}_{\psi_{b-}} = \begin{pmatrix}\mathcal{I}\\ \mathcal{O}\end{pmatrix}, \tag{4}$$

$$\begin{pmatrix}\mathcal{U}_2\\ \mathcal{V}_2\end{pmatrix}_{\psi_{b-}} = \begin{pmatrix}\mathcal{T}\\ \mathcal{I}\end{pmatrix}, \tag{5}$$

where $\mathcal{O}$ is the $M\times M$ zero matrix and $\mathcal{I}$ is the $M\times M$ unity matrix. Since the boundary conditions in equation (4) give $\delta\vec{B}\cdot\nabla\psi = 0$ at the liquid metal wall, these conditions correspond to a set of solutions that corresponds to the conducting wall type. On the other hand, since the boundary conditions in equation (5) guarantee the independent solutions to be continuous with the outer vacuum solutions, these conditions correspond to a set of solutions that corresponds to the no-wall type. Using the general expression for the solutions in equation (2), we can express the normal and parallel magnetic fields at the plasma–vacuum interface as follows:

$$\langle\mathcal{J}\nabla\psi\cdot\delta\vec{B}\rangle = -\mathcal{V}_1\boldsymbol{c}_{v1} - \mathcal{V}_2\boldsymbol{d}_{v1}, \tag{6}$$

$$-\langle\mathcal{J}\vec{B}\cdot\delta\vec{B}\rangle = \mathrm{i}\mathcal{K}_\parallel(\mathcal{U}_1\boldsymbol{c}_{v1} + \mathcal{U}_2\boldsymbol{d}_{v1}), \tag{7}$$

where $\mathcal{K}_\parallel = (\mathcal{M} - nq)\mathcal{I}$ and q is the safety factor.

Next, we describe the solution in the plasma region. The magnetic field line displacement $\vec{\xi}$ is introduced to represent the perturbed magnetic field $\delta\vec{B} = \nabla\times(\vec{\xi}\times\vec{B})$. On the plasma–vacuum interface at ψ_a, the normal magnetic field and the total pressure can be expressed as

$$\langle\mathcal{J}\nabla\psi\cdot\delta\vec{B}\rangle = \mathrm{i}\mathcal{K}_\parallel\langle\xi_\psi\rangle,$$

$$-\langle\mathcal{J}(\vec{B}\cdot\delta\vec{B} - \vec{\xi}\cdot\nabla P)\rangle = \mathcal{F}\langle\xi_\psi'\rangle + \mathcal{K}\langle\xi_\psi\rangle \equiv \langle w_p\rangle,$$

where $\xi_\psi = \nabla\psi\cdot\vec{\xi}$, a prime denotes a derivative with respect to ψ, and $\mathcal{F}$ and $\mathcal{K}$ are equilibrium matrices [13]. The equations describing the plasma region also can be solved by means of the independent solution method described in [13]. With M boundary conditions imposed at the magnetic axis, there remain only M independent solutions. The general solution can then be obtained as a combination of the M independent solutions,

$$\begin{pmatrix}\langle\xi_\psi\rangle\\ \langle w_p\rangle\end{pmatrix} = \mathrm{i}\begin{pmatrix}\Xi_p\\ \mathcal{W}_p\end{pmatrix}\boldsymbol{c}_p,$$

where the $M\times M$ matrices Ξ_p and $\mathcal{W}_p$ consist of the independent solutions, and $\boldsymbol{c}_p$ is a constant vector with M elements. Without loss of generality (by defining $\boldsymbol{c}_p = \Xi^{-1}\boldsymbol{c}_p^{\mathrm{new}}$ and $\mathcal{W}_p^{\mathrm{new}} = \mathcal{W}_p\Xi^{-1}$), we can set Ξ_p to be equal to $\mathcal{I}$. Therefore, we have

$$\langle\mathcal{J}\nabla\psi\cdot\delta\vec{B}\rangle = -\mathcal{K}_\parallel\boldsymbol{c}_p, \tag{8}$$

$$\langle\mathcal{J}(\vec{B}\cdot\delta\vec{B} - \vec{\xi}\cdot\nabla P)\rangle = \mathrm{i}\mathcal{W}_p\boldsymbol{c}_p. \tag{9}$$

The normal magnetic field component and the combined magnetic and thermal pressure are required to be continuous at the plasma–vacuum interface. Matching vacuum (equations (6) and (7)) and plasma (equations (8) and (9)) solutions at the interface ψ_a gives

$$\boldsymbol{d}_{v1} = \mathcal{F}_1^{-1}\delta W_b\delta W_\infty^{-1}\mathcal{F}_2\boldsymbol{c}_{v1}, \tag{10}$$

where $\delta W_\infty = \mathcal{W}_p - \mathcal{K}_\parallel[\mathcal{U}_2\mathcal{V}_2^{-1}]_{\psi_a}\mathcal{K}_\parallel$, $\delta W_b = \mathcal{W}_p - \mathcal{K}_\parallel[\mathcal{U}_1\mathcal{V}_1^{-1}]_{\psi_a}\mathcal{K}_\parallel$, $\mathcal{F}_1 = \mathcal{K}_\parallel[\mathcal{U}_2 - \mathcal{U}_1\mathcal{V}_1^{-1}\mathcal{V}_2]_{\psi_a}$ and $\mathcal{F}_2 = \mathcal{K}_\parallel[\mathcal{U}_1 - \mathcal{U}_2\mathcal{V}_2^{-1}\mathcal{V}_1]_{\psi_a}$. Note that δW_∞ and δW_b correspond to the energy integrals without a wall and with a perfectly conducting and non-rotating wall at ψ_b, respectively, as can be seen from equations (4) and (5).

We now consider the matching across the liquid metal wall and the error-field current layer. For the radial magnetic field, the Maxwell equation $\nabla\cdot\delta\vec{B} = 0$ and the thin layer assumption lead to

$$\langle v\rangle|_{\psi_{b-}} = \langle v\rangle|_{\psi_b} = \langle v\rangle|_{\psi_{b+}} = \boldsymbol{d}_{v1}. \tag{11}$$

The error-field current layer can cause a jump in the scalar magnetic potential:

$$\boldsymbol{J} \equiv \langle u\rangle|_{\psi_{b+}} - \langle u\rangle|_{\psi_b}, \tag{12}$$

where, $\boldsymbol{J}$ specifies the strength of the error field. The current in the liquid metal wall causes an additional jump in the scalar magnetic potential. This can be obtained from the liquid metal wall mode equation,

$$\boldsymbol{\nabla}\times\boldsymbol{\nabla}\times\delta\vec{B} = \mu_0\sigma\vec{V}\cdot\boldsymbol{\nabla}\delta\vec{B}, \tag{13}$$

where μ_0 is the vacuum permeability, σ is the wall conductivity and $\vec{V}$ is the liquid metal velocity. For simplicity, we assume that the liquid metal velocity is purely in the poloidal direction. In this case, equation (13) can be reduced to

$$\langle u\rangle|_{\psi_b} - \langle u\rangle|_{\psi_{b-}} = \mathrm{i}\mathcal{V}^{-1}\mathcal{V}_\theta\mathcal{M}\boldsymbol{d}_{v1}, \tag{14}$$

where $\mathcal{V}_\theta = [[\mu_0\sigma d\vec{V}\cdot\boldsymbol{\nabla}\theta/|\boldsymbol{\nabla}\theta|]]$ is the normalized velocity matrix, d is the wall thickness, and

$$\mathcal{V} = \mathcal{M}[[\mathcal{J}|\boldsymbol{\nabla}\psi||\boldsymbol{\nabla}\theta| - \mathcal{J}|\boldsymbol{\nabla}\psi\cdot\boldsymbol{\nabla}\theta|^2/(|\boldsymbol{\nabla}\psi||\boldsymbol{\nabla}\theta|)]] \times\mathcal{M} + n^2[[\mathcal{J}|\boldsymbol{\nabla}\phi|^2|\boldsymbol{\nabla}\psi|/|\boldsymbol{\nabla}\theta|]].$$

Since $\boldsymbol{c}_{v2} = 0$, we find that equations (2)–(5) yield

$$\langle u\rangle|_{\psi_{b+}} - \langle u\rangle|_{\psi_{b-}} = -\boldsymbol{c}_{v1}. \tag{15}$$

From equations (10), (12) and (14) we find

$$\boldsymbol{c}_{v1} = -\Lambda\boldsymbol{J}, \tag{16}$$

where

$$\Lambda = \mathcal{F}_2^{-1}\delta W_\infty(\mathrm{i}\mathcal{V}^{-1}\mathcal{V}_\theta\mathcal{M}\mathcal{F}_1^{-1}\delta W_b + \mathcal{F}_2^{-1}\delta W_\infty)^{-1}.$$

Finally, using equations (10), (11), (15) and (16), we obtain

$$\langle u\rangle|_{\psi_{b+}} - \langle u\rangle|_{\psi_{b-}} = \Lambda\boldsymbol{J}, \tag{17}$$

$$\langle v\rangle|_{\psi_{b+}} = \langle v\rangle|_{\psi_{b-}} = -\mathcal{F}_1^{-1}\delta W_b\delta W_\infty^{-1}\mathcal{F}_2\Lambda\boldsymbol{J}. \tag{18}$$

The torque on the liquid metal wall and the error-field current structure can be evaluated with the torque flux formula derived in [14],

$$\tau_\phi^e = \frac{1}{2}\int_{v_w} R^2\boldsymbol{\nabla}\phi\cdot\delta\vec{j}^*\times\delta\vec{B}\,\mathrm{d}v + cc = \frac{1}{2\mu_0}\left(\int_{\psi_{b+}} + \int_{\psi_{b-}}\right) R^2\delta\vec{B}^*\cdot\boldsymbol{\nabla}\phi\delta\vec{B}\cdot\mathrm{d}\vec{s} + cc, \tag{19}$$

where $\delta\vec{j}$ is the current density, R is the major radius, $\mathrm{d}v$ is the volume element, v_w denotes the volume occupied by the wall and the error field layer and $\mathrm{d}\vec{s}$ is the outward normal surface element vector surrounding the volume v_w. Torque in equation (19) can be reduced to

$$\tau_\phi^e = \frac{in\pi}{2\mu_0}(\langle u\rangle|^\dagger_{\psi_{b+}}\langle v\rangle|_{\psi_{b+}} - \langle u\rangle|^\dagger_{\psi_{b-}}\langle v\rangle|_{\psi_{b-}}) + cc.$$

Inserting equations (17) and (18), we obtain

$$\tau_\phi^e = -\frac{in\pi}{2\mu_0}\boldsymbol{J}^\dagger\Lambda^\dagger\mathcal{F}_1^{-1}\delta W_b\delta W_\infty^{-1}\mathcal{F}_2\Lambda\boldsymbol{J} + cc. \tag{20}$$

Without a liquid metal wall, we simply find $\Lambda = \mathcal{I}$. In this case we can see that τ_ϕ^e is inversely proportional to δW_∞ and has a singular-like peak at $\delta W_\infty \sim 0$. With the liquid metal wall introduced, however, Λ is proportional to δW_∞. This causes τ_ϕ^e to become directly—instead of inversely—proportional to δW_∞. The singular-like torque peak at $\delta W_\infty \sim 0$ without a liquid metal wall is therefore transformed into a vanishing minimum when a flowing liquid metal wall is present.

To understand this new result more clearly, let us first give the single mode expression for torque:

$$\tau_\phi^e = \frac{n\pi}{2\mu_0}|\boldsymbol{J}|^2|\Lambda|^2\frac{\mathcal{V}_1}{\mathcal{V}_2}\frac{\delta W_\mathrm{i}(\delta W_{b,\mathrm{r}} - \delta W_{\infty,\mathrm{r}})}{\delta W_{\infty,\mathrm{r}}^2 + \delta W_\mathrm{i}^2}, \tag{21}$$

where

$$\Lambda = [\delta W_{\infty,\mathrm{r}} + \mathrm{i}\delta W_\mathrm{i}][\delta W_{\infty,\mathrm{r}} + m\mathcal{V}_\theta(\mathcal{V}_1/\mathcal{V}_2\mathcal{V})\delta W_\mathrm{i} - \mathrm{i}[m\mathcal{V}_\theta(\mathcal{V}_1/\mathcal{V}_2\mathcal{V})\delta W_{b,\mathrm{r}} - \delta W_\mathrm{i}]]^{-1},$$

subscripts r and i represent the real and imaginary parts respectively and δW_i denotes the common imaginary part of δW_∞ and δW_b. Here and henceforth, we do not distinguish single mode matrix components from the corresponding matrix notations. In passing, we note that the key features of the liquid metal wall shielding effect do not change sensitively as the liquid metal wall crosses the ideal wall marginal position.

Next, let us consider the large-aspect-ratio limit with a circular cross section. We consider only a particular harmonic with poloidal mode number m. Imposing the boundary conditions in equations (4) and (5), we have

$$\mathcal{U}_1 = \frac{1}{2b^m}\left(r^m + \frac{b^{2m}}{r^m}\right), \qquad \text{for } \psi_a \leqslant \psi \leqslant \psi_{b-},$$

$$\mathcal{U}_2 = -\frac{b^m}{mRr^m}, \qquad \text{for } \psi_a \leqslant \psi \leqslant \psi_{b-} \text{ and } \psi_{b+} \leqslant \psi,$$

where r is the minor radius and b is the minor radius for the wall position. Since $\boldsymbol{c}_{v2} = 0$ in the outer vacuum region, $\mathcal{U}_1$ is not needed in this region. The plasma energy contribution can be written as

$$\mathcal{W}_p = -(w_\mathrm{mhd} + \mathrm{i}w_\mathrm{i})\frac{a}{mRb}(m - nq)^2,$$

where w_mhd and w_i represent the real and imaginary parts of the plasma energy normalized by the no-wall vacuum energy. In the shear Alfvén resonance case, w_i is roughly proportional to the toroidal rotation frequency Ω [7]. Also we can show that $-\mathcal{V}_1/\mathcal{V}_2|_{\psi_a} = (Rm/2)(1 - a^{2m}/b^{2m})$, where a is the plasma minor radius. Noting that $-|\boldsymbol{J}|^2\mathcal{V}_1^{-1}\mathcal{V}_2(\delta W_{b,\mathrm{r}} - \delta W_{\infty,\mathrm{r}})$ is positive, the torque in the cylindrical limit can be reduced to

$$\tau_\phi^e \propto -|\Lambda|^2\frac{w_\mathrm{i}}{(-w_\mathrm{mhd} + 1)^2 + w_\mathrm{i}^2}. \tag{22}$$

where

$$\Lambda = [-w_\mathrm{mhd} + 1 - \mathrm{i}w_\mathrm{i}][\mathrm{i}S\mathcal{V}_\theta(-w_\mathrm{mhd} + H - \mathrm{i}w_\mathrm{i}) - w_\mathrm{mhd} + 1 - \mathrm{i}w_\mathrm{i}]^{-1},$$

$H = [1 + (a/b)^{2m}]/[1 - (a/b)^{2m}]$ and $S = (a/b)^{2m}/2[1 - (a/b)^{2m}]$.

Equation (22) is plotted in figure 1 to display the dependence of the torque τ_ϕ^e (relative scale) on the negative plasma energy $-w_\mathrm{mhd}$. In the absence of a liquid metal wall, the torque is represented by the solid curves. Figure 1 shows that there is a steep peak in the torque around

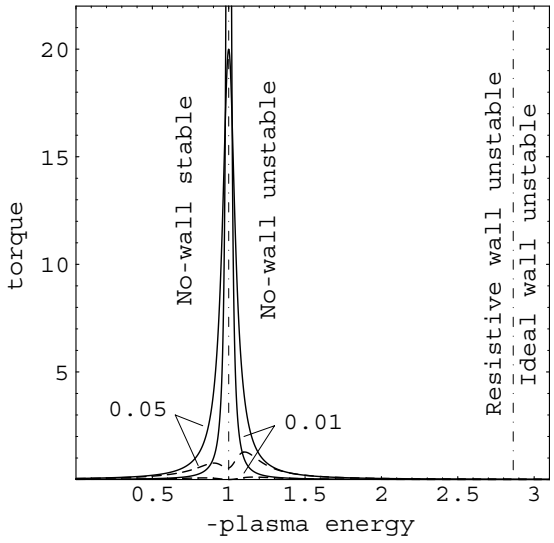

Figure 1. Dependence of the torque τ_ϕ^e on the negative plasma energy $w_{\rm mhd}$ for two different imaginary part energies $w_{\rm i}$: 0.01 and 0.05. The solid curves indicate the torque without the liquid metal wall. The dashed curves show the torque in the presence of the liquid metal wall. The maximum of the solid curve for $w_{\rm i} = 0.01$ extends to 200. The parameters are given as follows: $b = 1.2$, $v_\theta = 0.2$ and $m = 2$. The left vertical dot–dashed line represents the no-wall stability limit and the right one is the conducting-wall stability limit.

$w_{\rm mhd} = 1$ (i.e. the transition point for no-wall stability, $\Re e\{\delta W_\infty\} = 0$), which gives a strong torque barrier for plasma rotation. Furthermore, the smaller the rotation (i.e. smaller $w_{\rm i}$, for $w_{\rm i} \propto \Omega$ as in the shear Alfvén resonance case), the steeper the peak. This indicates that there is a self-enhancing synergistic sequence in plasma rotation braking. The error-field-created torque brakes the rotation. In return, the reduced rotation further enhances the strength of the braking torque. Consequently, an even stronger reduction of the plasma rotation is triggered. However, in the presence of the liquid metal wall (dashed curves), the magnitude of the peak is reduced dramatically. In particular, the reduction features the transformation of the torque maximum to a minimum at $\Re e\{\delta W_\infty\} = 0$. Furthermore, the liquid metal wall reverses the self-enhancing synergistic sequence in rotation braking. Smaller rotation now results in smaller torque on the plasma. In figure 1 the normalized speed of the liquid metal is $v_\theta = 0.2$, which is small and well within the technically achievable values.

In summary, we have shown that the error field can be shielded by a flowing liquid metal wall. The shielding effect is found to have these distinct features: a flowing liquid metal wall can prevent the resonance amplification of the error field by the plasma near its no-wall stability limit; moreover, it reverses the self-enhancing synergistic sequence in rotation braking. In this work we use the thin-wall approximation for simplicity. Some fusion reactor configurations propose to use thick flowing liquid metal blankets, which would lead to a similar shielding effect. It is interesting to point out that the flowing liquid metal wall can shield the error field, while providing simultaneously the stabilization effect on the resistive wall modes [15, 16].

We thank J.W. Van Dam for his helpful advice and comments on the current work. We also thank A. Boozer and M. S. Chu for helpful communication and discussion. This research was supported by the Office of Fusion Energy Science of the US Department of Energy under Grant DE-FG02-04ER54742.

References

[1] Freidberg J.P. 1987 *Ideal Magnetohydrodynamics* (Oxford: Clarendon)
[2] Strait E.J. *et al* 1995 *Phys. Rev. Lett.* **74** 2483
[3] Garofalo A.M. *et al* 1999 *Phys. Rev. Lett.* **82** 3811
[4] Sabbagh S.A. *et al* 2002 *Phys. Plasmas* **9** 2085
[5] Bondeson A. and Ward D.J. 1994 *Phys. Rev. Lett.* **72** 2709
[6] Betti R. and Freidberg J.P. 1995 *Phys. Rev. Lett.* **74** 2949
[7] Zheng L.-J., Kotschenreuther M. and Chu M. S. 2005 *Phys. Rev. Lett.* **95** 255003
[8] Boozer A.H. 2001 *Phys. Rev. Lett.* **86** 5059
[9] Fitzpatrick R. 2002 *Phys. Plasma* **9** 3459
[10] Garofalo A.M. *et al* 2002 *Phys. Plasmas* **9** 1997
[11] Gimblett C.G. and Hastie R.J. 2004 *Phys. Plasmas* **11** 1019
[12] Chance M.S. 1997 *Phys. Plasmas* **4** 2161
[13] Zheng L.-J. and Kotschenreuther M. 2006 *J. Comput. Phys.* **211** 748
[14] Boozer A.H. 2003 *Phys. Plasmas* **10** 1458
[15] Gimblett C.G. 1989 *Plasma Phys. Control Fusion* **31** 2183
[16] Umansky M.V., Betti R. and Freidberg J.P. 2001 *Phys. Plasmas* **8** 4427